Optimal Power Utilization by Adjusting Torque Boost and Field Weakening Operation in Permanent Magnet Traction Motors

Konstantinos I. Laskaris, *Member, IEEE*, and Antonios G. Kladas, *Member, IEEE*

***Abstract*—Variable speed traction systems require constant adaptation of torque and speed, and thus, it is desirable to reduce motor size and weight by approximating constant power curve as much as possible. The design strategies under which a permanent magnet motor can demonstrate significant torque over-boost and field weakening capabilities using single-gear transmission are investigated. This paper gives a good quantitative comparison of surface-mounted, internal, and hybrid rotor topologies, featuring permanent magnets by introducing a power utilization coefficient, which benchmarks the capability of a traction system to utilize its rated power over the whole speed range, while optimal transmission ratio is investigated for the three rotor topologies.**

***Index Terms*—Field weakening control, finite-element methods, gear design, permanent magnet motors, sinusoidal back-EMF, torque boost.**

NOMENCLATURE

$V_{\rm dc}$	Battery pack dc voltage.
B_n	Normal magnetic flux density component.
T_m	Mechanical torque.
T_w	Wheel mechanical torque.
$P_{\rm nom}$	Nominal motor mechanical power.
$V_{\rm max}$	Maximum vehicle speed.
ω_o	Minimum angular speed limit.
$\omega_{\rm max}$	Angular speed that vehicle reaches $V_{\rm max}$.
PUC	Power utilization coefficient.

I. INTRODUCTION

PERMANENT magnet (PM) motors became favorable in the automotive industry in the past few years, due to their advantages of high efficiency, high power density, and high drive performance [1]. To further improve the performance of electric power train, recent efforts have also been concentrated on the motor design and analysis by applying numerical techniques for accurate parameter prediction and dynamic model development [2], [3].

Mounting wheel motors to the electric vehicle (EV) in order to minimize transmission losses during accelerating or regenerative braking has been very promising, as described in [4]. However, in high performance EVs, it is difficult to obtain high power compaction without rotating at high speed, which can only be achieved, if a transmission gear interferes. In such cases, the main target is to maximize the product of torque and speed, by ensuring sufficient over-torque capability for limited time intervals [5]–[7].

Single-gear transmission has been preferable over conventional use of clutch and gearbox in electric traction systems, as they can produce high starting torque and flexibility in delivering torque. Contrarily, an internal combustion engine is unable to produce starting torque, while torque at low speed is very low. These are the main reasons that a gearbox and clutch has always been required in order to adapt torque and speed and efficiently utilize the available power. Some disadvantages of gearbox use are the high transmission losses, delay time during gear transition that reduces performance, as well as complicated mechanical construction that requires maintenance. However, the inarguable advantage of a gearbox is the excellent capability to adapt mechanical power either by increasing torque and lowering speed or vice versa. This gives an excellent utilization of the available power that dramatically increases vehicle performance, in order to avoid traction system oversizing; however, the use of gearbox has an impact on efficiency.

As these advantages of the gearbox cannot be neglected, recent research introduced continuous variable transmission (CVT) systems in hybrid EVs that eliminated some of the traditional gearbox drawbacks. CVTs can gradually modify transmission ratio allowing the motor to operate only at a desirable speed range. However, CVT systems are expensive, not as efficient as conventional gearboxes and add more complicated control to the traction system [8]–[10]. Magnetic gear, an alternative to CVT, mainly adopted in wheel motor design, proposed in [11] and [12], allows adequate tradeoff between torque and speed. However, overall efficiency declines and, for this reason, is not widely preferred in high power systems. A double rotor variation is proposed in [13] that improves the machine efficiency and increases the torque density.

A single-gear traction motor has to deliver multiple times the torque of the multigeared motor and multiple times the rotating speed. By taking into account these specs, the single-gear motor results in being huge, in order to deliver this torque and inefficient in high-speed operation. Under this condition, can a single-gear electric traction system approximate the performance of a multigear?

Manuscript received August 31, 2011; revised January 20, 2012; accepted February 20, 2012. Date of publication May 8, 2012; date of current version July 27, 2012. Paper no. TEC-00461-2011.

The authors are with the Laboratory of Electrical Machines and Power Electronics, National Technical University of Athens, Athens 15780, Greece (e-mail: laskaris@central.ntua.gr; kladasel@central.ntua.gr).

This research has been co-financed by the European Union (European Social Fund - ESF) and Greek national funds under the General Secretariat for Research and Technology of Greece Program: 09-51-988 - "Development of electric bus prototype".

Digital Object Identifier 10.1109/TEC.2012.2194741

The answer is "yes," but specific motor design and control strategies have to be applied in order to achieve such performance. In a variable speed drive of an EV, driving performance requires high mean mechanical power over the whole speed range. This is translated as highest possible torque at low speed and highest possible speed keeping constant power. Ideally, the maximum mechanical power available can be delivered at any rotating speed. In this way, the ideal torque curve is a hyperbolic function of speed.

By appropriately programming the over-torque capability of the motor, the size can be limited down, but similar strategy has to be done in the high-speed area to allow efficient high-speed operation. Excitation adjustable machines, such as synchronous motors featuring rotor windings and induction motors, have a significant advantage of either weakening the field in high speed or strengthening it at very low speed to provide efficient high rotation or increased torque, respectively. In this way, they can perform, under conditions, as bigger or faster motors. The inarguable advantage of PM motors is that they provide excitation magnetic field without sacrificing power losses associated with excitation windings [4]. On the other hand, such an excitation magnetic field is not adjustable causing significant iron losses and requiring very high phase voltage feed at high speed. This specific drawback raises the question, under which conditions a PM motor can be superior to an induction or separately excited synchronous motor, for variable speed drives [14], [15]. This paper aims to demonstrate the design strategies under which a PM motor can preserve significant torque over-boost (ToB) advantages and adequate field weakening (FW) capability. The topology which can perform as close to constant power is investigated further in this paper.

II. PM Motor Configuration Analysis

A. Design Considerations

As a general rule, ToB and FW are mutually exclusive. A strong magnetic loading can deliver increased torque levels but will be very difficult to weaken at high rotating speed.

Surface mounted PM motors have been considered to be poor candidates for achieving wide constant power operation by means of flux weakening. If the flux linkage is reduced, it also reduces the torque capability [4], [16]. In counterparts, internal PM machines present a certain inherent flux weakening capability increased with loading current that is why they are more suitable for these applications [17].

The configurations adopted are four-pole/three-phase motors, sharing the same stator design. Stator outer diameter is 250 mm and rotor diameter is 126 mm, while active motor length is 150 mm. The air gap radial length is 0.6 mm. The stator consists of 12 slots featuring full pitch distributed windings and is manufactured from laminated M-19, 0.35-mm-thickness, silicon steel that has been processed to minimize core losses. Stator has been designed to deliver high levels of electric loading without being saturated. This has been done by considering low magnetic flux density in stator teeth (1.4 T), in normal operation that will not exceed 2 T under high current boost [17].

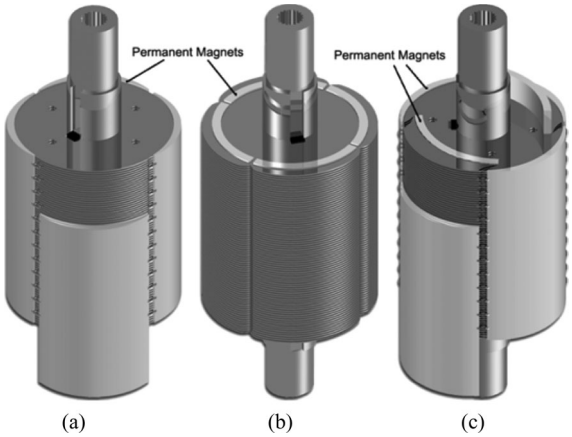

Fig. 1. (a) Surface PM rotor. (b) Internal PM rotor. (c) Hybrid PM rotor.

At this point, a critical decision has to be made in order to decide the magnetic loading introduced by the PMs involved. Three rotor designs are being investigated in order to evaluate their ToB and FW capability and check their suitability to approximate the ideal hyperbolic torque curve that is the most favorable. The sinusoidal back-EMF waveform demonstrates high efficiency over a wider speed range and is adopted in all rotor designs.

Rotor ***A*** [see Fig. 1(a)] features surface mounted PMs, the shape of which has been optimized to provide sinusoidal flux density distribution in the air gap and thus sinusoidal back-EMF waveform. The magnets (N42SH) are alternately poled, magnetized through their small dimension, and can tolerate up to 150 °C operating temperature. PMs are firmly mounted on the laminated core by using tips in a percentage of 20% of the total sheets, which provides adequate mounting reliability up to 8000 r/min. The flux leakage due to the PM mounting tips is less than 0.02% and thus will be neglected in the finite-element analysis that follows.

Rotor ***B*** [see Fig. 1(b)] features constant width, internally mounted PMs (N45SH). Iron core is laminated to reduce eddy currents and the shape has been optimized in order to produce sinusoidal field distribution, similarly to Rotor ***A***. Main characteristics of this rotor is the relatively high flux leakage due to the iron core outside the PMs that sacrifices some magnetizing flux to provide increased weakening capability, as subsequently demonstrated.

Finally, rotor ***C*** [see Fig. 1(c)] is a hybrid surface/internal PM rotor that is a good candidate of providing enhanced torque boost characteristics compared to rotor ***A***, by using increased volume of PM material. Moreover, torque ripple is higher due to the even order harmonics as the consequent magnet poles are not identical, but does not affect designing at this point as torque ripple is less than 5% due to the sinusoidal back-EMF [18]. Surface PMs have been mounted similarly to Rotor ***A***, while additional internal PMs have been employed to reinforce the magnetic field, having same magnetization direction with their respective neighboring surface PM. The laminated core features holding tips, as in rotor ***A*** and furthermore, optimized shape

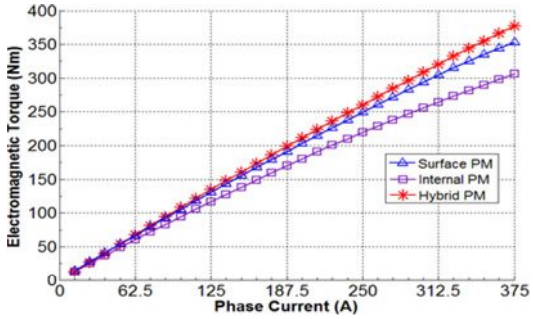

Fig. 2. Simulated electromagnetic torque with phase current.

internal slots to reduce the flux leakage to the internal PMs and provide sinusoidal field distribution.

A 2-D finite-element model has been employed to analyze the motor configurations. Sensitivity analysis was performed in order to decide on critical design parameters to maximize efficiency, driving torque, speed range, and to minimize active part size [4], [16]. The geometry optimization of the motor enables us to achieve a convenient compromise between the two important parameters of performance and efficiency. The next sections analyze the ToB and FW capability of the aforementioned topologies.

B. ToB Operation

The ToB capability is determined by the stator at first place. The more the magnetic circuit stays unsaturated under current over-boost, the more linearly torque increases, as shown in Fig. 2. In all rotor cases considered, the stator is the same, and thus, in terms of electric loading, the capabilities are common for all three motor configurations. High torque cannot be applied for a long time interval on a moving system, as high acceleration will soon end up when top speed is reached. The worst case scenario for an EV, that requires high torque for the longest time interval, is a steep slope start with full thrust. This is the maximum loading condition in which the traction system of a small passenger EV can be found.

Specifically, the constant current value is 125 A and current boosting can increase up to 150% of the rated value (180 A) for 50 s or up to 200% of the rated value (250 A) for 30 s. These time intervals have been determined experimentally in Section III using temperature monitoring. The heat sink that the stator carries is capable of dissipating 2.0 kW of heat with free ventilation at ambient temperature.

Fig. 2 shows the electromagnetic torque curve variation with stator current for the three rotor cases. This figure illustrates that the saturation effects are relatively small as the torque varies almost linearly with loading. Simulation has been done for higher values than the prescribed to demonstrate the saturation level of the magnetic circuit. However, stator current will never exceed 250 A under any loading condition. The highest torque capability has been achieved by rotor ***C*** (hybrid topology). This is mainly due to the important interpole reluctance obtained by the relatively large PM volume. Rotor ***A*** (Surface PM) performance is similar to rotor ***C*** (hybrid) but in high current values is quite inferior. Rotor ***B*** (internal PMs) demonstrates the lowest torque capability, compared to the other cases. This is mainly due to the increased flux leakage that the outer part of rotor core causes.

This leakage is further increased with loading current. Higher grade PMs, N45SH, have been employed instead of N42SH to compensate with the flux leakage. The result of this leakage can also be observed by comparing the electromotive forces (EMF) of the three cases, shown in Fig. 5. EMF values of ***A*** and ***C*** are similar but the one from ***C*** is quite lower.

Fig. 3 shows the flux density distribution under maximum ToB (250 A) for the three rotors adopted. Rotors ***A*** and ***C*** demonstrate similar field distribution in the magnetic circuit, while in Rotor ***B*** case, the local magnetic flux accumulation with loading in the rotor core limits down the capacity of the motor to produce torque. Core saturation not only increases the iron losses [4] but also makes stator current less capable of producing torque [17].

C. FW Operation

In PM variable speed drive, high rotating speed is limited due to two main reasons.

1) The first reason is the high voltage developed by excitation field. An inverter has limitations in increasing phase voltage, due to the limited $\boldsymbol{V}_{\mathrm{dc}}$ of the battery pack. If the motor reaches this limit, it cannot rotate faster.
2) The second reason is the high iron loss developed as speed grows. Iron losses constitute almost a second-order polynomial of speed that increases motor temperature and downgrades the efficiency significantly.

FW control aims to suppress excitation field in order to reduce back-EMF and iron losses at the same time. Actually, under FW operation, there is a tradeoff between copper and iron losses. From an efficiency point of view, it is worth spending some power in copper losses to reduce the magnetic flux density in the air gap, which will subsequently cause reduced iron losses at high speed. However, this consideration is accurate only when taking into account the field fundamental frequency suppression. As demonstrated further in this section, higher harmonics, however, can be a dominant factor in iron losses and particular attention has to be paid in this respect.

Fig. 4 shows the magnetic flux density distribution for the three rotor cases. Fig. 4(a) and (c) shows FW operation under 80% of the nominal stator magnetomotive force (MMF) at zero torque angle $\boldsymbol{I_d}$, while Fig. 4(b) shows the FW operation under 30% of the stator nominal MMF.

The clear advantage of the interior permanent magnet (IPM) motor is that the excitation field is suppressed utilizing much less MMF compared to rotor ***A*** and ***C***, while much lower mean value of $\boldsymbol{B_n}$ is achieved in the air gap. This is mainly because it is inevitable to weaken the excitation field without providing a leakage path to the magnetic flux, other than that of the stator, at the designing phase. This path is more important in rotor ***B*** which mainly consists of the iron core outside the PMs shown in Fig. 4(b). A thick outer core part will allow better FW due to the increased flux leakage, but will downgrade the torque that the motor is capable of, under normal or ToB operation. Additionally, the thicker the PM, the harder to

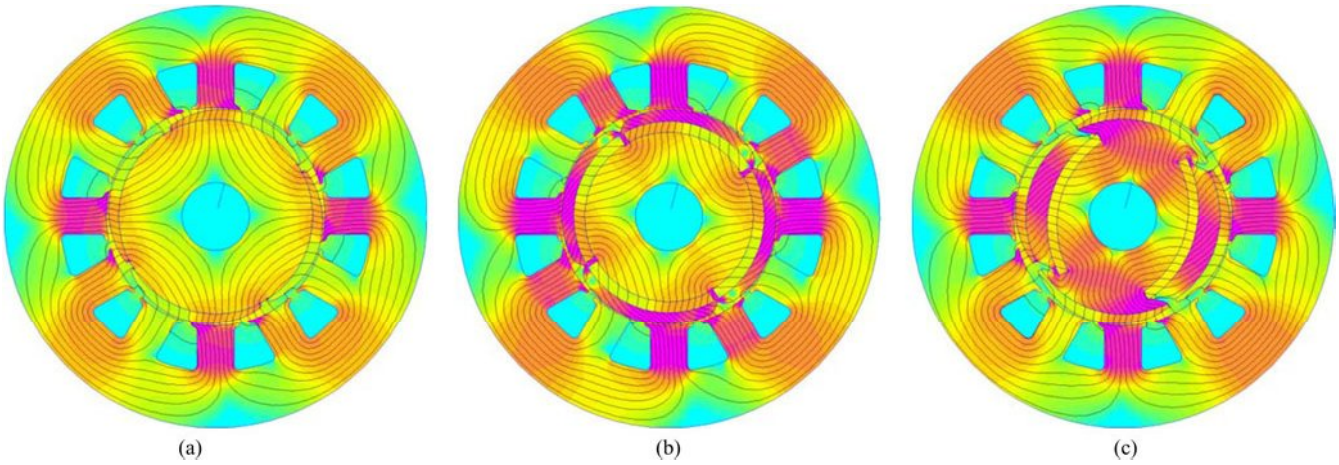

Fig. 3. Magnetic flux density distribution under maximum torque boost operation. (a) Surface magnet rotor. (b) Internal constant width magnet rotor. (c) Hybrid surface/internal magnet rotor.

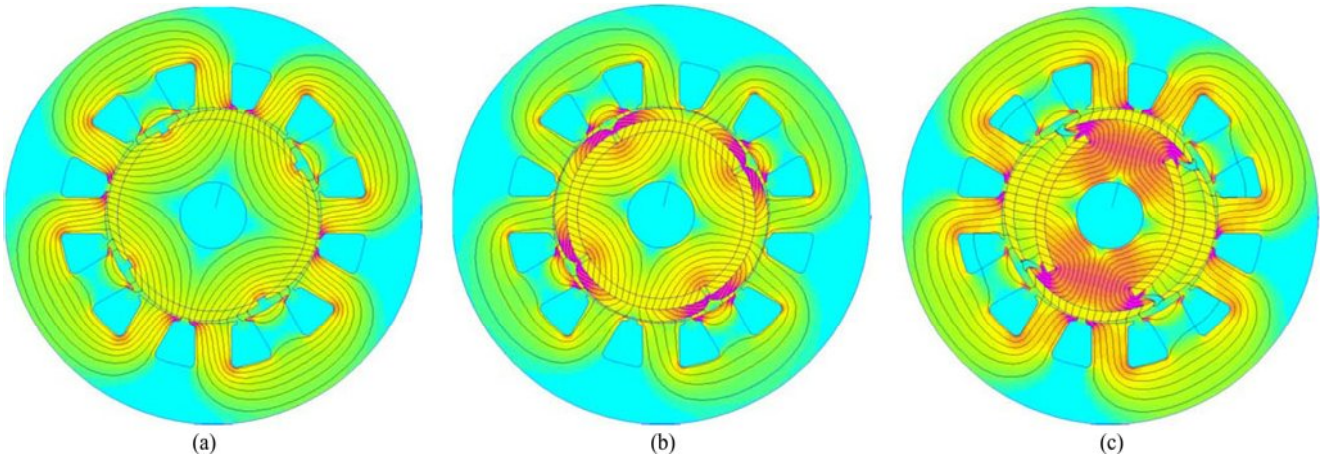

Fig. 4. Magnetic flux density distribution under maximum FW operation. (a) Surface magnet rotor (80% MMF). (b) Internal constant width magnet rotor (30% MMF). (c) Hybrid magnet rotor (80% MMF).

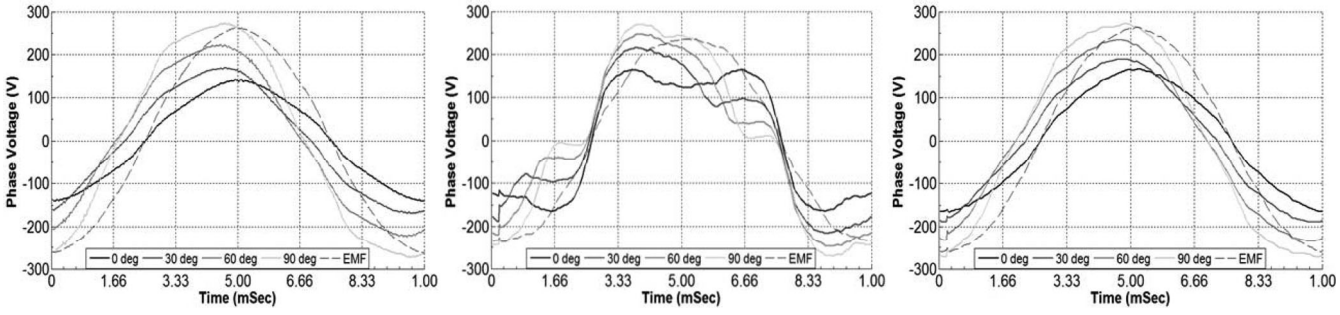

Fig. 5. Simulated voltage at 200 Hz (6000 r/min) with different torque angle.

weaken the field, but the highest ToB capability it provides. Fig. 5 shows the EMF of each of the three rotors along with the gradual phase voltage reduction when operating under FW control.

Phase voltage shown in Fig. 5 derives by applying the respective MMF in various torque angles. According to Fig. 5 legend, 0° respects to the zero torque angle, while 90° respects to the optimal torque angle.

In order to estimate core losses, a methodology that quantizes the area into square elements is adopted [18]. This methodology tracks the variation of magnetic flux density for every square element over a full cycle and derives the specific hysteresis and eddy current loss components. Then, the respective core losses are computed by integrating over the active motor length. Fig. 6 illustrates the iron loss distribution in the stator and rotor, for the FW operation, which plays very important role, regarding

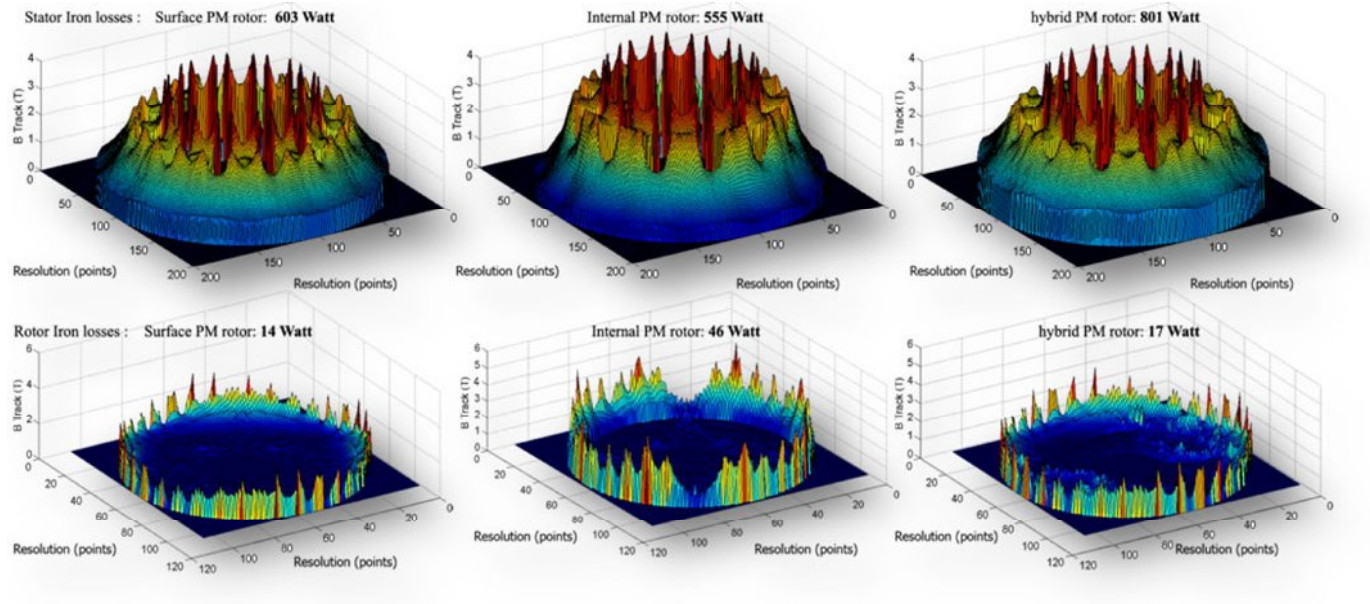

Fig. 6. Simulated iron loss distribution for the three rotors adopted under FW operation (200 Hz).

PM thermal demagnetization protection, as FW operation takes place at steady state.

It has to be noted that case ***B*** has a drawback when weakening the field to the limits, as high harmonic components appear. The magnetic flux fluctuates in the rotor iron core when moving from one stator tooth to the next and thus rotor iron losses increase with loading current. Rotor iron losses are due to minor hysteresis loops and are less significant than stator iron losses, as shown in Fig. 6. However, it is very important to keep rotor core losses low, as rotor overheating could cause demagnetization of the PMs.

In the upper row in Fig. 6, iron loss distribution in the stator yoke is much lower for the IPM rotor, as the fundamental frequency is significantly suppressed compared to the other rotor cases. However, higher harmonics cause increased losses on the stator teeth, which justifies the absolute values of stator iron losses. Rotor losses are higher for the internal PM rotor, due to the fluctuation of the magnetic flux density in the outer rotor core part; however, the values are acceptable, considering the much higher weakening capability that IPM provides, as demonstrated in the experimental validation.

By observing iron losses for the three cases considered, it is obvious that the IPM has an advantage in FW operation due to the comparatively lower iron losses introduced, which allows more efficient high-speed operation. However, at ToB operation, the highest efficiency is expected to be achieved by the hybrid rotor topology, as iron losses are nearly similar to the surface rotor topology, but torque delivered is higher. An efficiency comparison between the three topologies under 27-kW constant power control is performed in the next section.

Fig. 7 illustrates the three prototype rotors that have been manufactured in order to validate the simulated results experimentally.

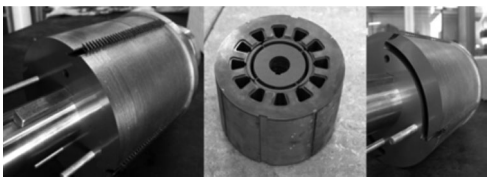

Fig. 7. Three rotor prototypes prior to mounting the PMs.

III. Experimental Validation

The presented simulation results have been validated by measurements obtained on a convenient experimental setup.

The PM motors have been mounted on a separately excited, 150-kW DC motor to validate the drive system performance (see Fig. 8). The dc converter driving the DC motor is a four quadrant +/−420-V, 280-A converter that either provides positive or negative mechanical power for propulsion or regenerative braking operation. A custom made three-phase insulated gate bipolar transistor (IGBT) inverter, 600 V/300 A is being driven by a digital signal processing board that receives input from the rotor position, the throttle position (torque request), the temperature sensor arrays from the motor, IGBTs and battery pack, and the dc voltage of the battery, to provide with appropriate PWM drive.

The dc voltage comes from a $LiFePO_4$ battery pack, that consists of 144 cells, each capable of 3.2 V/20 Ah. The battery pack is 460 V/20 Ah, weighs 110 kg, and is able to provide 9.2 kWh, enough energy to move the Smart for-two experimental vehicle for about 110 km in an average urban environment. However, the battery pack is the main bottleneck of the power system, as electric power is limited to 32 kW constant and 60 kW burst for 30 s. For this reason, constant power control has been adapted to the limitations of the battery system.

Fig. 8. Experimental setup.

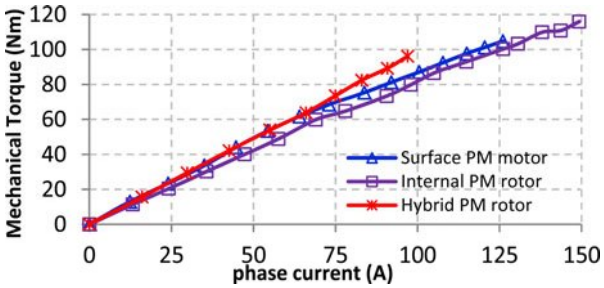

Fig. 9. Measured mechanical torque with phase current for the three rotors.

Measurements have been performed by using programmable multichannel oscilloscope. A piezoelectric sensor mounted on the stator housing of the DC motor has been used in order to map mechanical torque into voltage. The measured characteristic torque curves of the three cases are illustrated in Fig. 9. As expected from the simulation results, the hybrid PM rotor provides the steepest torque curve and gives almost linear torque variation with phase current.

Surface PM rotor delivers comparatively lower torque as current increases due to the thin outer part of the PMs. Finally, the internal PM rotor gives the lowest torque due to the increased flux leakage in the rotor core.

Fig. 10 illustrates the measured efficiency of each motor case under constant torque constant power control. Hybrid PM rotor achieves the highest efficiency, but due to the higher magnetic loading and reduced FW capability, efficiency inclines with speed. A better efficiency over wider speed range is achieved by using the surface PM rotor, and finally, the internal PM rotor allows significantly enhanced efficiency at high-speed operation. This is mainly due to the mean magnetic flux density reduction in the stator core. However, although the total losses are kept at reasonable values, even at that high speed, iron losses tend to increase rotor temperature, and this justifies using high-temperature PMs for FW operation.

In order to demonstrate each rotor FW capability, an experiment where the inverter dc voltage has been limited to 60 V, in order to constrain maximum speed, was performed. Fig 11 illustrates the no load maximum angular speed versus $\boldsymbol{I_d}$ current, which gives a comparative FW capability of the three rotors. Copper losses have been plotted in the same diagram to indicate the impact on efficiency, of using $\boldsymbol{I_d}$ current to weaken the PM field. The highest EMF suppression has been achieved for the internal PM rotor as simulated in Section II-C. This allows significantly higher rotating speed by utilizing only a small fraction

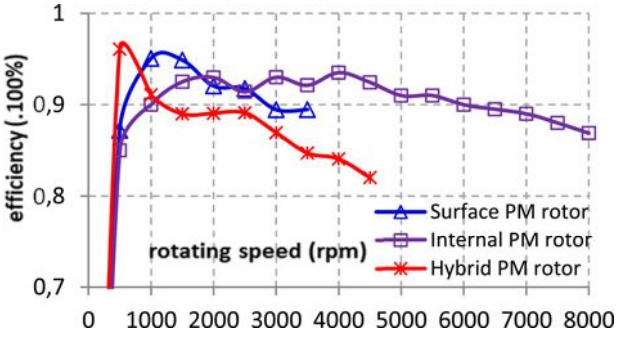

Fig. 10. Measured efficiency with speed for constant power 27 kW.

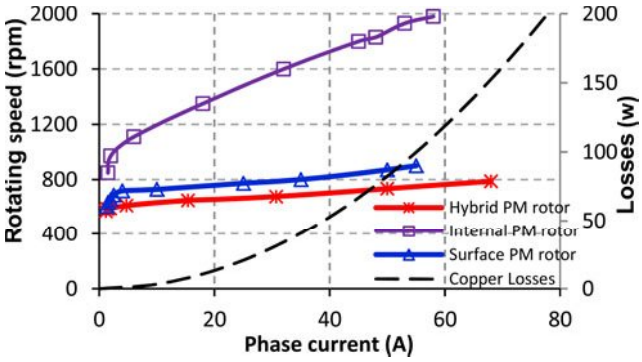

Fig. 11. FW capability under $V_{\rm dc} = 60$ V.

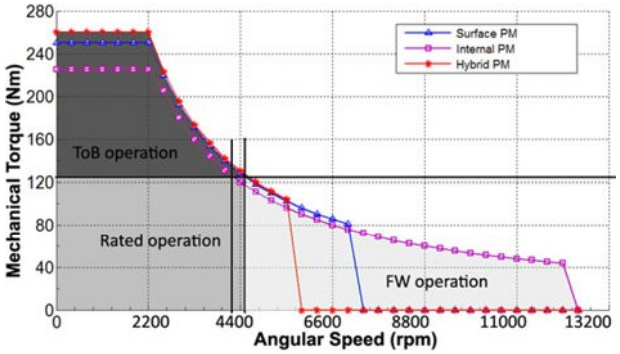

Fig. 12. Measured mechanical torque with rotor speed for the three rotors.

of the nominal MMF. Contrarily, hybrid and surface PM rotors demonstrated poor FW capability as back-EMF reached soon the maximum level that the inverter could provide for the 60-V dc voltage.

In Fig. 12, the three operation areas, *ToB*, *Rated,* and *FW* are shaded in different gray tone. These curves have been measured by keeping stator current at 250 A at ToB operation and gradually decreasing it so that constant nominal power is preserved. FW control begins when the motor reaches its rotating limits from a back-EMF point of view. Furthermore, PM losses due to switching frequency harmonics cause additional losses on surface PMs. This is further enforced by the low mean inductances due to PMs. In order to minimize PM losses, a high switching frequency (12 kHz) has been adopted.

Motor specifications are tabulated in Table I, while further results are included in Section V.

TABLE I
MOTOR CHARACTERISTICS AND SPECIFICATIONS

QUANTITY	SURFACE PM ROTOR GEOMETRY	INTERNAL PM ROTOR GEOMETRY	HYBRID PM ROTOR GEOMETRY
Rated Mechanical Power	60 kW *(80 HP)*	56 kW *(75 HP)*	61 kW *(82 HP)*
Continuous Torque	128 Nm	120 Nm	130 Nm
Maximum phase voltage	300V	300V	300V
Torque Boost Capability	250.0 Nm *(for 30 sec)*	225.0 Nm *(for 30 sec)*	260.0 Nm *(for 30 sec)*
Speed range	0 - 6900 rpm	0 - 12000 rpm	0 - 5500 rpm
Field Weakening control	Over 4500 rpm	Over 5000 rpm	Over 4300 rpm
Power compaction factor	1,21 HP/kg	1,13 HP/kg	1,23 HP/kg

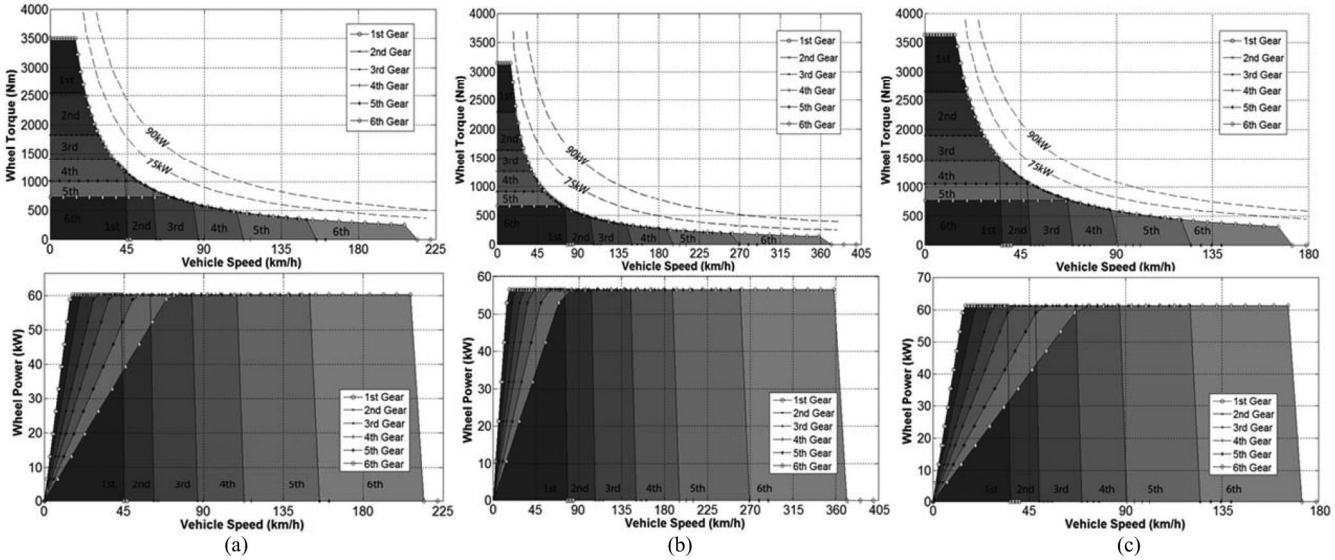

Fig. 13. Wheel torque and power with vehicle speed using available gears. (a) Rotor A-surface PM rotor. (b) Rotor B-internal constant width PM rotor. (c) Rotor C-hybrid surface/internal PM rotor.

IV. COMPARATIVE ANALYSIS

A. PUC

The lack of gearbox requires increased torque performance from motors in EV traction applications at low speed ranges, resulting in the development of constant power control strategies proposed [4]. A less powerful traction system can, under some conditions, provide significantly better performance to the EV due to the good power utilization. The work introduces a PUC that is defined as the fraction of the mean power in the whole speed range, during acceleration, over the nominal power of the traction system:

$$\mathrm{PUC} = \frac{1}{P_{\mathrm{nom}}} \cdot \frac{1}{(\omega_{\max} - \omega_0)} \cdot \int_{\omega_0}^{\omega_{\max}} T_m(\omega) \cdot \omega \, d\omega. \quad (1)$$

Ideal PUC is equal to unity and represents a traction system that can provide hyperbolic wheel Torque with speed. PUC is multiplied by the rated system power to indicate the actual available power that determines an EV performance. As deriving from the above, the PUC is dependent on the combined operation of the motor with the transmission ratio. The ideal hyperbolic torque curve, which is used as reference, gives a respective constant rectangular power curve (see the first and second rows in Fig. 13, respectively). The more torque curve approaches the hyperbolic curve, the better the PUC.

TABLE II
AVAILABLE TRANSMISSION RATIOS AND EFFICIENCY

1st Gear	14.00 : 1	91%
2nd Gear	10.18 : 1	93%
3rd Gear	7.29 : 1	93%
4th Gear	5.59 : 1	93%
5th Gear	4.06 : 1	94%
6th Gear	2.94 : 1	94%

B. Optimal Gear Ratio and PUC Classification

An electric motor has to demonstrate very good ToB and FW characteristics so that it can give performance close to a traction system with gearbox. In any other case, motor overdimensioning is required so that it can provide adequate driving performance. It can be noted that a motor that performs very well in flux weakening area can tradeoff with ToB by selecting a shorter gear. Similarly, a motor that is more capable of tackling with high torque rather than high and efficient speed will be combined to a longer transmission ratio. In order to choose one out of the six available gears for each case, the following two considerations are taken into account: In a passenger car, an average tire on an average road surface gives a friction factor that allows approximately 1300 Nm of torque per wheel, before it loses traction and starts spinning. This means that for a two wheel drive, boosting wheel torque over 2600 Nm is

TABLE III
TRACTION SYSTEM AND VEHICLE SPECIFICATIONS

QUANTITY	ROTOR *A*	ROTOR *B*	ROTOR *C*
Rated Power	60 kW *(80 HP)*	56 kW *(75 HP)*	61 kW *(82 HP)*
PUC	0.81	0,86	0.77
Max Wheel Torque	1299 Nm	1525 Nm	981 Nm
Max Vehicle Speed	108 km/h	145 km/h	127 km/h
Mean Power over speed range	45.198 kW	44.73 kW	43.68 kW
Transmission ratio	5.59 : 1 (best *PUC*)	7.29 : 1 (best *PUC*)	4.06 : 1 (best *PUC*)

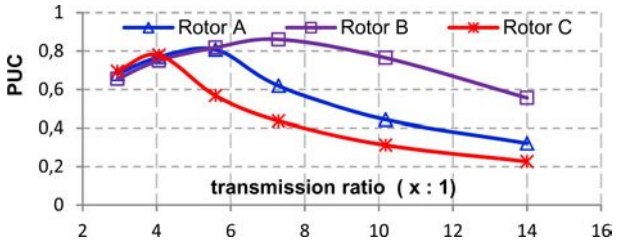

Fig. 14. Optimal PUC investigation with transmission ratio.

minor, if not meaningless, even for sport performance vehicles. For this reason, the gear ratio has to enable high wheel torque; however, higher than 2600 Nm would be a waste. Moreover, as aerodynamic friction losses constitute a second-order polynomial of speed, vehicle speed has to be constrained so that good utilization of the available energy is achieved, in order to be able to drive a reasonable distance. In this study, the vehicle adopted is a small city car, and thus, speed constraint is set to 120 km/h. Some gear ratios can theoretically give much higher speed, sometimes far from feasible, as in Fig. 13(b), but the speed range taken into account will be up to 120 km/h. Under these two constraints, the gear ratio that gives the highest PUC and delivers the highest driving performance is investigated for each rotor case.

The first row in Fig. 13 illustrates the wheel torque developed by combining the three PM motor measured torque curves in Fig. 12 with the available gear ratios in Table II. Table II also includes the respective single-gear efficiency, for each gear. Each gear provides a compromise between high torque and high speed. The second row in Fig. 13 illustrates the mean power tradeoff between low- and high-speed operations. Surfaces shaded in common gray tone define the energy gain for each gear, during acceleration. PUC improves by increasing this active power surface either way.

Highest utilization is achieved by the internal PM rotor [see Fig. 13(b)], where the high-speed operation allows use of very short transmission ratio and thus providing very high wheel torque. Furthermore, surface PM rotor, due to rotation limitation, needs longer transmission ratio to provide the vehicle with adequate end up speed (area of 120 km/h), and this leads to a compromise with torque [see Fig. 13(a)]. Finally, the hybrid topology gives the worst PUC, as the higher ToB cannot make up for the poor FW capability, requiring even longer transmission ratio. According to Fig. 14 and Table II, the optimal selection for rotor ***A*** is the fourth gear (5.59:1), for rotor ***B*** is the third gear (7.29:1), and for rotor ***C*** is the fifth gear (4.06:1).

Fig. 14 illustrates the calculated PUCs for the three rotor cases. For each rotor case, there is an optimal gear ratio that gives maximum PUC, delivering maximum mean power. Table III gives comparative characteristics of the traction systems analyzed in this study. By appropriate rotor configuration design and by appropriately selecting transmission ratio, a good PUC and thus a good approximation of the hyperbolic curve can be achieved that can keep motor oversizing at reasonable level.

V. CONCLUSION

This paper approached electric traction motor design by appropriately configuring rotor geometry and subsequently choosing the optimal gear ratio, in order to transfer maximum possible mechanical power over the whole driving speed range. A surface-mounted, an internal, and a hybrid rotor topology, featuring PMs, was studied and compared for their suitability to approximate the ideal hyperbolic torque curve, using single-gear transmission, by evaluating their torque boost and FW capability.

In order to classify these topologies, a PUC was introduced that provided benchmark to evaluate the combined use of an electric traction system together with a specific single-gear transmission. Simulation results and measured ones were in good agreement in all cases considered. Such a comparison enabled not only to verify the well-known IPM suitability for variable speed drive, but also focused on the quantitative advantages and disadvantages that each of the topologies adopted provides in performance and efficiency. The IPM prototype has replaced the previous SPM prototype, adopted in [17] and [18], as it provided the best option from a driving characteristics point of view, as tabulated in Table III.

REFERENCES

[1] H. Grotstollen, "Optimal design of motor and gear drives with high acceleration by consideration of torque-speed and torque-acceleration product," *IEEE Trans. Ind. Appl.*, vol. 47, no. 1, pp. 144–152, Jan./Feb. 2011.
[2] T. Ohnishi and N. Takahashi, "Optimal design of efficient IPM motor using finite element method," *IEEE Trans. Magn.*, vol. 36, no. 5, pp. 3537–3539, Sep. 2000.
[3] D. J. Sim, D. H. Cho, J. S. Chun, H. K. Jung, and T. K. Chung, "Efficiency optimization of interior permanent magnet synchronous motor using genetic algorithms," *IEEE Trans. Magn.*, vol. 33, no. 2, pp. 1880–1883, Mar. 1997.
[4] K. Laskaris and A. Kladas, "Internal permanent magnet motor design for electric vehicle drive," *IEEE Trans. Ind. Electron.*, vol. 57, no. 1, pp. 138–145, Jan. 2010.

[5] S. Stoicovy, "Geared versus gearless adjustible-speed drive systems in the pulp and paper industry," *IEEE Trans. Ind. Appl.*, vol. 24, no. 4, pp. 641–648, Jul./Aug. 1988.
[6] K. Rahman, N. Patel, T. Ward, J. Nagashima, F. Caricchi, and F. Crescimbini, "Application of direct-drive wheel motor for fuel cell electric and hybrid electric vehicle propulsion system," *IEEE Trans. Ind. Appl.*, vol. 42, no. 5, pp. 1185–1192, Sep./Oct. 2006.
[7] Y. Yang and D. Chuang, "Optimal design and control of a wheel motor for electric passenger cars," *IEEE Trans.*, vol. 43, no. 1, pp. 51–61, Jan. 2007.
[8] M. Itoh, K. Hayasaka, and M. Yamanaka, "Modelling and simulation of shaft drive CVT: Study on characteristic of ratio change mechanism," in *Proc. IEEE Int. Conf. Mechatron. Autom.*, Jun. 25–28, 2006, pp. 979–983.
[9] L. Xu, Y. Zhang, and X. Wen, "Multioperational models and control strategies of dual-mechanical-port machine for hybrid electric vehicles," *IEEE Trans. Ind. Appl.*, vol. 45, no. 2, pp. 747–755, Mar./Apr. 2009.
[10] S. Savaresi, F. Taroni, F. Previdi, and S. Bittanti, "Control system design on a power-split CVT for high-power agricultural tractors," *IEEE/ASME Trans. Mechatronics*, vol. 9, no. 3, pp. 569–579, Sep. 2004.
[11] L. Wang, J. Shen, P. Luk, W. Fei, C. Wang, and H. Hao, "Development of a magnetic-geared-magnet brushless motor," *IEEE Trans. Magn.*, vol. 45, no. 10, pp. 4578–4581, Oct. 2009.
[12] K. Chau, D. Zhang, J. Jiang, C. Liu, and Y. Zhang, "Design of a magnetic-geared outer-rotor permanent-magnet brushless motor for electric vehicles," *IEEE Trans. Magn.*, vol. 43, no. 16, pp. 2504–2506, Jun. 2007.
[13] R. Qu and T. Lipo, "Design and parameter effect analysis of dual-rotor radial-flux, toroidally wound, permanent-magnet machines," *IEEE Trans. Ind. Appl.*, vol. 40, no. 3, pp. 771–779, May/Jun. 2004.
[14] W. Soong and N. Ertugrul, "Field weakening performance of interior permanent-magnet motors," *IEEE Trans. Ind. Appl.*, vol. 38, no. 5, pp. 1251–1258, Sep./Oct. 2002.
[15] F. Caricchi, F. Crescimbini, F. Mezzetti, and E. Santini, "Multistage axial-flux PM machine for wheel direct drive," *IEEE Trans. Ind. Appl.*, vol. 32, no. 4, pp. 882–888, Jul./Aug. 1996.
[16] A. Refaie, "Fractional-slot concentrated-windings synchronous permanent magnet machines: Opportunities and challenges," *IEEE Trans. Ind. Electron.*, vol. 57, no. 1, pp. 107–121, Jan. 2010.
[17] K. Laskaris and A. Kladas, "High performance traction motor design and construction for small passenger electric car," presented at the Proc. XVIV Int. Conf. Electr. Mach., Rome, Italy, Sep. 6–9, 2010, Paper ID 1428.
[18] K. Laskaris and A. Kladas, "Permanent magnet shape optimization effects on synchronous motor performance," *IEEE Trans. Ind. Electron.*, vol. 58, no. 9, pp. 3776–3783, Sep. 2011.

Konstantinos I. Laskaris (M'09) was born in Greece in 1978. He received the Diploma degree in electrical and computer engineering from the National Technical University of Athens, Athens, Greece, in 2002, and the M.Sc. degree in communications and signal processing from the Faculty of Electrical and Electronic Engineering, Imperial College London, London, U.K. He is currently working toward the Ph.D. degree in the Department of Electrical and Computer Engineering, National Technical University of Athens.

His research interests include permanent magnet machine modeling and applied field weakening techniques for electric vehicle motor optimal efficiency control.

Mr. Laskaris is a member of the Technical Chamber of Greece.

Antonios G. Kladas (M'87) was born in Greece in 1959. He received the Diploma degree in electrical engineering from the Aristotle University of Thessaloniki, Thessaloniki, Greece, in 1982, and the DEA and Ph.D. degrees from the University of Pierre and Marie Curie, Paris, France, in 1983 and 1987, respectively.

He was an Associate Assistant in the University of Pierre and Marie Curie from 1984 to 1989. During 1991–1996, he was with the Public Power Corporation of Greece, where he was involved in the System Studies Department. Since 1996, he has been with the Department of Electrical and Computer Engineering, National Technical University of Athens, Athens, Greece, where he is currently a Professor. His research interests include transformer and electric machine modeling and design, as well as analysis of generating units by renewable energy sources and industrial drives.

Dr. Kladas is a member of the Technical Chamber of Greece.